JOINT EUROPEAN TORUS JET

JET–P(93)15

S. Migliuolo

Ion Temperature Gradient Modes and Impurities in Toroidal Shaped Plasmas

Ion Temperature Gradient Modes and Impurities in Toroidal Shaped Plasmas

S. Migliuolo[1]

JET-Joint Undertaking, Culham Science Centre, OX14 3DB, Abingdon, UK

[1]Permanent address: Research Laboratory of Electronics, Massachusetts Institute of Technology, Cambridge, Massachusetts, USA.

Preprint of a paper to be submitted for publication in Nuclear Fusion
March 1993

ABSTRACT

The linear theory of electrostatic instabilities driven by ion temperature gradient is investigated for impure plasmas in shaped (e.g., elliptical and triangular) toroidal plasma cross-sections. Kinetic theory is used to describe the response of each ion species. Both even and odd parity branches of these "ITG" modes [B. Coppi and F. Pegoraro, *Nucl. Fusion* 17, 969, 1977] are examined in detail for parameters relevant to high temperature experiments. The Shafranov shift tends to lower the growth rates of both nodes, most notably that of the odd parity mode. Ellipticity in the plasma cross section has a strong stabilizing effect on the even parity mode, but leaves the odd parity mode essentially unaffected. Triangularity has a much weaker (also stabilizing) effect and can be ignored, for practical situations. Strong stabilization by multiply charged impurities is encountered, primarily due to dilution of the primary ion concentration.

1. INTRODUCTION

Since the original discovery [1] of the instability of the Ion Temperature Gradient (ITG) mode, much work has been carried out to study the linear stability properties of these drift-type instabilities. Both the slab branch (whose instability requires compression of the ion fluid in the direction parallel to the magnetic field; this compressibility couples the drift wave to the ion sound wave) [2]-[12] and the toroidal branch (driven by the compressibility of the perpendicular $\mathbf{E}\times\mathbf{B}$ ion drift; this manifests itself by the appearance of the precession drift velocity) [13]-[26] have received attention in the literature. Both branches appear to have the lowest threshold for instability (generally expressed by the ratio of the temperature gradient scale length to another characteristic length, e.g., the density scale length, $\eta_i = L_n / L_T$, or the toroidal major radius, $\varepsilon_T = L_T / R$) when the effective perpendicular wavelength is of the order of an ion Larmor radius ($k_\theta \rho_i \approx 1$, where $\rho_i = \sqrt{2T_i m_i}\, c / eB$). The instability also generally manifests itself at long parallel wavelengths, $k_\parallel L_n << 1$.

If we denote the relative importance of these two branches by the ratio of frequencies that characterise the two compression processes, $\Re = \omega_{di} / k_\parallel v_{Ti}$, where $\omega_{di} = 2k_\theta c T_i / eBR = (L_n / R)\omega_{*i}$, we see that $\Re = k_\theta \rho_i (L_n / R) / k_\parallel L_n$ is generally greater than unity, when $k_\theta \rho_i \approx 1 (\Re \approx (L_n / R) k_\parallel L_n > 1$, since $L_n / R \approx 1/4 - 1/3$, typically) and the toroidal branch is dominant in Tokamak experiments (at least insofar as modes with finite growth rate are concerned).

Since ITG modes have long been considered to play an important role in the process of anomalous energy loss in Tokamaks (see, e.g., Refs. [27]-[29] for experimental evidence), it is of importance that the linear stability properties of these modes be determined by models that reproduce experimental situations as closely as possible. Thus, one aim of the present work is to examine the theory of plasmas with non-circular cross-sections.

In addition, recent experiments [30]-[32] have called into question the relevance of ITG modes in toroidal experiments by finding no appreciable change in energy transport characteristics , as the theoretically predicted thresholds (in η_i or ε_T) were crossed. Tentative explanations for this disagreement have included (1) the possibility that "rule of thumb" thresholds are too crude to accurately portray the experiments and that more precise analysis must be carried out for each shot [33], (2) that the theory is wrong and that the ITG threshold is really determined by a dominant trapped ion term [34]. While both proposal have merit, we wish to recall that the ITG threshold can be radically altered by the presence of impurities. This was first pointed out in Ref. [35], explored further in Refs. [36]-[37] (slab branch) and [38]-[39] (toroidal branch). Recently, local calculations have produced the claim [40]-[41] that the actual instability thresholds, computed for impure plasmas, are actually much higher (by factor of 2-8, depending on the perpendicular wavelength of the mode) than those for pure plasmas, bringing theory in line with these experiments. Thus, we also consider a multi-ion plasma (with all species considered kinetic) and study the effect of impurities on the ITG instability with a fully non-local calculation. Throughout this paper, we assume equal temperatures for all species, for simplicity.

2. EQUILIBRIUM

The condition for equilibrium is the well-known Grad-Shafranov equation for the poloidal flux fiction, ψ:

$$\frac{\partial^2\psi}{\partial r^2}+\frac{1}{r}\frac{\partial\psi}{\partial r}+\frac{1}{r^2}\frac{\partial^2\psi}{\partial\theta^2}-\frac{1}{R}\left(\cos\theta\frac{\partial}{\partial r}-\frac{1}{r}\sin\theta\frac{\partial}{\partial\theta}\right)\psi = \tag{1}$$

$$=-4\pi R^2\frac{dP}{d\psi}-F(\psi)\frac{dF}{d\psi}$$

where P = plasma pressure, $R = R_0 + r\cos\theta$ is the major radius ($R_0 \leftrightarrow$ magnetic axis), θ and ϕ are the poloidal and toroidal co-ordinates and $F = RB_\phi$. The

poloidal magnetic field is related to the flux function by $\mathbf{B}_p = \nabla\psi \times \nabla\phi$. The equilibrium is assumed to be axisymmetric (independent of ϕ). We consider the case of a low-β equilibrium with F = constant and P having a parabolic dependence on the flux function (this is well satisfied in, e.g., JET). We thus define:

$$B_1 = 2\pi R_0^2 \left.\frac{dP}{d\psi}\right|_{\psi=0} , \quad \frac{1}{r_B^2} = 4\pi R_0^2 \left.\frac{d^2P}{d\psi^2}\right|_{\psi=0} \tag{2}$$

We use $\varepsilon = r/R_0 << 1$ as an expansion parameter. We refer the reader to Freiberg's book [42] for a description of techniques and cases of solution of this Eq.. To zeroth order in ε, the Grad-Shafranov Eq. reads:

$$\frac{\partial^2\psi_0}{\partial r^2} + \frac{1}{r}\frac{\partial\psi_0}{\partial r} + \frac{1}{r^2}\frac{\partial\psi_0}{\partial\theta^2} = -2B_1 - \frac{\psi_0}{r_B^2} \tag{3}$$

Notice that in this way we build ellipticity and triangularity into the equilibrium independently from toroidal corrections. The lowest order flux function is expanded into harmonics:

$$\psi_0 = \sum_m H_m(r)\ \cos\ m\theta \tag{4}$$

Since Eq. (3) is separable, each harmonic can be solved for independently:

(i) m = 0 harmonic:

$$H_0(r) = -2B_1 r_B^2\left[1 - J_0(r/r_B)\right] \tag{5}$$

(ii) $m \geq 1$ harmonics:

$$H_{m\geq 1}(r) = -2B_1 r_B^2 \delta_m J_m(r/r_B) \tag{6}$$

where δ_m is constant denoting the relative strength of the harmonic.

To first order in the toroidal correction, the Eq. for the equilibrium reads:

$$\frac{\partial^2\psi_1}{\partial r^2}+\frac{1}{r}\frac{\partial\psi_1}{\partial r}+\frac{1}{r^2}\frac{\partial^2\psi_1}{\partial\theta^2}+\frac{\psi_1}{r_B^2}= \\ =\frac{1}{R_0}\left(\cos\theta\frac{\partial}{\partial r}-\frac{1}{r}\sin\theta\frac{\partial}{\partial\theta}\right)\psi_0-2\frac{r}{R_0}\cos\theta\left(2B_1+\frac{\psi_0}{r_B^2}\right) \tag{7}$$

Substitute for ψ_0 from Eq. (4)-(6) and defining the dimensionless variable $x = r / r_B$, the following equation is obtained:

$$\frac{\partial^2\psi_1}{\partial x^2}+\frac{1}{x}\frac{\partial\psi_1}{\partial x}-\frac{1}{x^2}\frac{\partial^2\psi_1}{\partial\theta^2}=-\left(\frac{r_B}{R}\right)\left(2B_1r_B^2\right)\left\{\cos\theta\left[(J_1+2xJ_0)+\frac{1}{2}\delta_2(J_1-2xJ_2)\right]\right. \\ +\cos2\theta\left[\frac{1}{2}\delta_3(J_2-2xJ_3)\right]+\cos3\theta\left[-\frac{1}{2}\delta_2(J_3+2xJ_2)\right] \\ \left.+\cos4\theta\left[-\frac{1}{2}\delta_3(J_4+2xJ_3)\right]\right\} \tag{8}$$

Once again, each harmonic in θ can be obtained independently, expanding $\psi_1(x,\theta)=\sum h_m(r)\cos m\theta$. A set of Eq.s, written symbolically as $L_n h_n(x) = xM_n$, where $L_n(x)\equiv x\left[d^2/dx^2+(1/x)d/dx+\left(1-n^2/x^2\right)\right]$ and M_n is the coefficient of the cos nθ harmonic of the right side of Eq. (8). These can be formally solved via Green's function techniques, where the Green's function corresponding to the n-th harmonic is:

$$G_n(x,y)=-\frac{\pi}{2}\left[J_n(x)Y_n(y)H(y-x)+Y_n(x)J_n(y)H(x-y)\right] \tag{9}$$

where J_n and Y_n are Bessel functions of the first and second kind respectively and H is Heavyside's step function. Thus, the formal solution $h_m(r)=-\int_0^x dy\ yG(x,y)M(y)$ can be evaluated in principle (here X is a free parameter, which is adjusted so as to give no contribution from the homogeneous solution of $Lh_m(x)=0$). For example, we show the pure toroidal correction (i.e., neglecting contributions of order $\varepsilon\delta_m << 1$, which represent the coupling between toroidicity and non-circularity):

$$\psi_1(x)=\frac{\pi B_1 r_B^3}{R}\left\{Y_1(x)\left[J_0^2(x)-4\sum_{k=0}^{\infty}\left((k+1)J_{2k+2}^2(x)+(2k+1)J_{2k+1}^2(x)\right)\right]\right.$$
$$\left.+J_1(x)\left[-xY_1(x)J_0(x)+\frac{1}{2}\sum_{k=0.1}x^{k+2}\left(J_0(x)Y_k(x)+J_1(x)Y_{k+1}(x)\right)\right]\right\} \qquad (10)$$

In what follows we specialise in an equilibrium of zero order in ε and keep only ellipticity (m = 2 in Eq. (4)), apart from one case study in which we will vary triangularity , and one where the effect of the toroidal correction (Shafranov shift) will be discussed. This is motivated by a desire to explore the linear stability of the inner portion of the plasma column, where triangularity (m = 3) is very small, for low-β experiments (small Shafranov shift). The neglect of terms of order ε is not crucial for modes with high poloidal wavenumber. The Jacobian of the transformation of co-ordinates (from r, θ, and ϕ to ψ, θ, and ϕ) is then:

$$J=\frac{1}{|\nabla\psi\times\nabla\phi\cdot\nabla\theta|}=\frac{rR_0}{2B_1 r_B}\left\{J_1\left(\frac{r}{r_B}\right)+\delta_2\left[J_1\left(\frac{r}{r_B}\right)-2\frac{r}{r_B}J_2\left(\frac{r}{r_B}\right)\right]\cos 2\theta\right\}^{-1} \qquad (11)$$

Using this Jacobian, we can define an inverse rotational transform (i.e. a generalised "q(r, θ)"):

$$q(r,\theta)=\int^{\theta}d\theta'\left(\frac{rB_\phi}{RB_\theta}\right)_{\psi\,=\,const}=\int^{\theta}d\theta'\left(\frac{J}{R^2}\right)_{\psi\,=\,const}\approx\frac{B_o}{2B_1}\int^{\theta}d\theta'\left(\frac{r}{r_B}\right)_{\psi\,=\,const} \qquad (12)$$
$$\times\left\{J_1(r/r_B)+\delta_2\left[J_1(r/r_B)-2\frac{r}{r_B}J_2(r/r_B)\right]\cos 2\theta'\right\}^{-1}$$

where the subscript ψ = const indicates that the minor radius is to be taken over a constant -ψ flux surface. The toroidal magnetic field at the magnetic axis is denoted by B_0. Thus, we can relate the constant B_1 to q_0, the equivalent cylindrical inverse rotational transform at the magnetic axis (take the limits $r/rB\to 0$ and $\delta_2=0$ in Eq. (12)): $q_0=B_0/B_1$. Similarly, the scale length r_B can be related to the edge value of the equivalent cylindrical q(r), by using $B_\theta=-(1/R)(\partial\psi)(\partial r)$ in $q(r=a)\approx aB_\phi/RB_\theta=(B_0/2B_1)(a/r_B)(1/J_1(a/r_B))$ in the cylindrical case. One thus obtains the transcendental equation $2(r_B/a)J_1(a/r_B)=q_0/q(a)$ which can be solved for $r_B=f(a,q_0,q(a))$.

The ellipticity of the equilibrium, at a given flux surface ψ, can be computed easily:

$$k_{ell} = \frac{2r(\psi,\theta=\pi/2)}{r(\psi,\theta=0)+r(\psi,\theta=\pi)} \approx \sqrt{\left.\frac{2+\delta_2}{2-\delta_2}\right|_{r<<r_B}} \tag{13}$$

3. ANALYTIC LINEAR THEORY

In order to introduce some salient features of the instability due to ion temperature gradients and precession drifts, we focus on a simple limit: that of fluid-like modes (whose frequency is much larger than the precession drift frequency) that are strongly ballooning (i.e., have a maximum at $\theta = 0$ and decay very fast away from it) in a plasma with circular cross section. The dispersion equation for electrostatic modes can be written as:

$$\left\{\frac{d^2}{d\theta^2}+\left(\frac{qR\omega}{c_s}\right)\left[\frac{\omega+\omega_{*i}}{\omega-\omega_{*i}(1+\eta_i)}-\frac{\varpi_{di}}{\omega}\left(\cos\theta+\hat{s}\theta\sin\theta\right)+\bar{b}_i\left(1+\hat{s}^2\theta^2\right)\right]\right\}\hat{\phi} \tag{14}$$

where $\hat{\phi}(\theta)$ is the amplitude of the perturbed electrostatic potential (i.e., the potential is $\tilde{\phi}(r,\theta,\phi)=\hat{\phi}(\theta)\ \exp\ iS$, where $\mathbf{B}\cdot\nabla S = 0$), $\varpi_{di} = 2k_\theta cT_i / eBrR$ is the precession drift frequency (it arises from the compression of the $\mathbf{E}\times\mathbf{B}$ drift), $\omega_{*i} = k_\theta cT_i / eBrL_n$ is the ion diamagnetic frequency, $\eta_i = L_{ni} / L_{Ti}$ is the ion temperature gradient parameter, $\bar{b}_i = k_\theta^2 T_i / m_i\Omega_i^2$ represents the finite Larmor radius (FLR) parameter, $c_s = \sqrt{T_e / m_i}$ is the sound speed, and qR plays the role of a parallel wavelength (more precise definitions of all these quantities will be given in the next chapter). The variable θ represents both the poloidal angle as well as the coordinate parallel to the magnetic field (note that $\mathbf{B}\cdot\nabla\hat{\phi} = \exp(iS)\left(B_p / qR\right)d\hat{\phi}/d\theta$). This dispersion equation can be derived directly from fluid theory (cf. [20]), or from kinetic theory (by taking the limits $|\omega| >> \varpi_{di}$ and $k_\perp\rho_i << 1$). Since it has been used extensively in the literature, we present it without derivation .

By considering strongly ballooning modes, we can expand the harmonic functions about $\theta = 0$: $\cos\theta \approx 1-\theta^2/2$, $\sin\theta \approx \theta$ and obtain a Weber-type equation which can be solved analytically. The resulting dispersion relation is:

$$\left(\frac{qR\omega}{c_s}\right)^2\left[\frac{\omega+\omega_{*i}}{\omega-\omega_{*i}(1+\eta_i)}-\frac{\varpi_{di}}{\omega}+\bar{b}_i\right]=(2N+1)\sigma \tag{15}$$

where

$$\sigma=\pm\left(\frac{qR\omega}{c_s}\right)\left[\frac{\varpi_{di}}{\omega}\left(\hat{s}-\frac{1}{2}\right)-\bar{b}_i\right]^{1/2} \tag{16}$$

and where N is the radial mode number (i.e., order of the Hermite polynomial); the choice of sign in Eq. (16) is dictated by the requirement that the mode be spatially localized. Note that our Eq. (15), is the same as Eq. (14) of Ref. [22], as expected.

One comment worth making at this point concerns the parity of the mode under consideration. Even parity modes (i.e., modes that have $\hat{\phi}(-\theta)=\hat{\phi}(\theta)$) can be driven unstable both by the ion temperature gradient and by the precession of trapped electrons, they have been studied [43] under the appellation of "ubiquitous modes". The odd parity modes (also considered in Ref. [43]) are not affected by trapped electrons (to lowest order in the ratio of mode frequency to electron bounce frequency) and, thus, are purely η_i-type modes. In this study, we choose to disregard the effect of trapped electrons, so as to isolate the consequences of the presence of two ion populations, each with a temperature gradient.

The dispersion relation, Eq. (15)-(16), can be cast as a fifth order polynomial in ω/ω_{*i}. An interesting limit occurs for $(c_s/qR\omega_{*i})^2\left[(\hat{s}-1/2)(r_n/R)-\bar{b}_i\right]<<1$, when the sound wave decouples from the toroidal η_i mode (the ion temperature gradient instability).

The resulting dispersion relation has the solution:

$$\frac{\omega}{\omega_{*i}}=\frac{1}{2(1+\bar{b}_i)}\left\{\left(-1+\varepsilon+\bar{\eta}\bar{b}_i\right)\pm\left[\left(-1+\varepsilon+\bar{\eta}\bar{b}_i\right)^2-4\varepsilon\bar{\eta}\left(1+\bar{b}_i\right)\right]^{1/2}\right\} \tag{17}$$

where $\varepsilon\equiv 2r_n/R$ (the ratio of the density gradient scale length to the major radius) and $\bar{\eta}=1+\eta_i$. This solution is the same as that from the local theory (in

the small b_i, fluid-like limit). Note that the unstable mode can rotate in the electron diamagnetic direction (for small $\overline{\eta}\bar{b}_i$, cf. [20]-[23]). This is a feature of our fluid limit that permits an instability even at small values of $\overline{\eta} \equiv 1+\eta$ (i.e., $\eta_i < 0$!), whereas kinetic theory will show the mode to be stabilized at finite positive values of η_i (due to Landua or precession drift damping). Still, it is interesting to see an "ion" mode propagating in the electron drift wave direction. Also, not that the solution of Eq. (17) predicts that an instability of the toroidal branch exists only for a range of temperature gradients: $\eta_- \le \overline{\eta} \le \eta_+$ where $\eta_\pm$ are the roots for the zero of the discriminant in Eq. (17).

Solutions of Eq. (15)-(16) are presented in Fig. 1. We recover the known result (from the description of the slab branch in sheared geometry, cf. [2] and [44]) that modes with moderate N grow strongest (i.e., not the fundamental but, rather, the N = 5 - 10 harmonics) and see that the coupling to the sound wave tends to broaden the η_i interval in which the mode is unstable (for $\bar{b}_i = 0.1$ and $\varepsilon = 0.25$, Eqs. (17) predicts instability for $0.24 \le \eta_i \le 2.36$). Indeed, as η_i increases to large values, the mode becomes more slab-like and the instability of the slab branch tends to dominate over that of the toroidal branch (for these particular choices of parameters, $\bar{b}_i = 0.1, 0.25$, which denote long perpendicular wavelength modes). This can be seen analytically by ordering $\eta_i >> 1$ and $\omega / \omega_{*i} < \eta_i$ in Eqs. (15)-(16), while taking (for example) $1 < \varepsilon / \bar{b}_i < (2N+1)^2 \left(c_s / qR\omega_{*i}\right)^2 / \bar{b}_i$ in Eq. (17). The resulting cubic in the frequency always has an unstable root (the growth rate of this fluid-like instability has an asymptotic value that is independent of η_i).

The solution of Eq. (14), namely the fluid limit without the strong coupling approximation, is show in Fig. 2, for both the even and odd parity modes. One can see a clear trend toward stabilization by (small values of) the FLR parameter (at constant ω_{*i}). Also, we note that the modulation of the precession drift frequency results in a lowering of the growth rate, showing that the toroidal ITG mode is primarily driven by the θ component of the precession drift (the term that carries the cos θ factor in Eq. (14)). Once again, the odd mode is somewhat more unstable than the even mode. Note that $\omega / k_\parallel v T_i \approx (\omega / \omega_{*i})\ \omega_{*i} qR / \sqrt{2} c_s \approx (\omega / \omega_{*i}) \sqrt{\bar{b}_i} R / L_n$ is much larger than unity only for finite values of η_i, in Fig. 2, indicating that our ordering fails for small η_i and that the slab branch will dominate the behaviour of the long wavelength modes near marginal stability.

4. LINEAR KINETIC THEORY

The modes of interest are high poloidal mode number drift-type waves (as discussed in the introduction, we are looking at regimes where $k_\theta \rho_i \sim 1$) in equilibria with finite magnetic shear. Hence, the well-known "ballooning formalism" [45] is appropriate here. We refer the reader to Refs. [46]-[47] for a detailed derivation of the equations governing linear stability. Here we simply not that the formalism considers modes that are localised near a mode rational surface, whose principal structure perpendicular to the equilibrium magnetic field is that of a plane wave $(k_\perp >> k_\parallel)$ and which have a variation along the magnetic field with a maximum at $\theta = 0$ (even "ballooning" modes) or at $|\theta| = \theta_0 \leq \pi / 2$ (odd "ballooning" modes). Periodicity of the eigenfunction in the poloidal direction requires that the physical eigenfunction be constructed through the superposition of the aforementioned plane waves, leading to the so-called "ballooning representation". A transformation of the governing equations to conjugate space leads to the final dispersion equation (in the electrostatic limit, or set of equations in the electromagnetic limit) expressed in terms of a single angle-like variable, known as the "extended" poloidal variable [45]. For practical purposes this simply entails replacing θ by this extended variable in the governing equations and extending the space from $(-\pi,\pi)$ to $(-\infty,\infty)$.

The mode parallel phase velocity is taken to be larger than the ion thermal speed $\omega > \omega_{di} \geq k_\parallel v_{Ti}$, cf. the introduction) and much smaller than the electron thermal speed. Hence, the electron response is purely adiabatic $\left(\tilde{n}_e = e\tilde{\phi} n_e / T_e\right)$, while we can safely ignore trapped ion effects. Trapped electron contributions are disregarded, as noted earlier, in order to isolate the "pure" η_i variant of the ITG mode. In real life, trapped electrons will influence the even parity branch of the toroidal ITG mode. The dispersion equation that governs linear stability then is (cf. [47]):

$$\left(1+\sum_{j\neq e}\frac{T_j}{T_e}\frac{Z_j^2 n_j}{n_e}\right)\frac{e\hat{\phi}(\theta)}{T_e}-\sum_{j\neq e}\frac{Z_j^2}{n_e}\frac{T_j}{T_e}\int d^3v\frac{\omega-\omega_{*j}^T}{\omega-\omega_{Dj}}$$

$$\left(J_0^2(\Theta)-J_0(\Theta)v_\parallel\hat{b}\cdot\nabla'\frac{v_\parallel}{\omega-\omega_{Dj}}\hat{b}\cdot\nabla'\frac{1}{\omega-\omega_{Dj}}J_0(\Theta)\right)\frac{e\hat{\phi}(\theta)}{T_e}=0 \qquad (18)$$

where $\hat{b}\cdot\nabla' = (1/JB_0)(d/d\theta)$ is the effective parallel wavenumber (from now on θ denotes the "extended poloidal variable"), $\hat{b}$ is the unit vector in the direction parallel to the equilibrium magnetic field, the energy dependent diamagnetic frequency is

$$\omega_{*j}^{T} = \omega_{*j}\left[1-\eta_j\left(\frac{3}{2}-\frac{E}{T_j}\right)\right],\ \omega_{*j} = -\frac{T_j}{m_j\Omega_j}\hat{b}\times\nabla S\cdot\nabla \ln n_j \tag{19}$$

while the precession drift frequency (function of energy E and magnetic moment μ) is

$$\omega_{Dj} = \omega_{dj}\frac{E-\mu B/2}{T_j},\ \omega_{dj} = \frac{2T_j}{m_j\Omega_j}\hat{b}\times\nabla S\cdot\vec{k} \tag{20}$$

note that we use the low-β definition of the precession drift frequency (see, e.g., Refs. [48]-[49] for the general definition). The magnetic curvature vector is defined by $\vec{k} = \hat{b}\cdot\nabla\hat{b}$, while the eikonal S, whose gradient defines the lowest order perpendicular wavevector, is: $S = n[\phi - q(r,\theta)]$ with q defined in Eq. (12) and n being the toroidal wavenumber. The wavevector ∇S can then be evaluated in any coordinate system, e.g. (r,θ,ϕ), using the expression for ψ. The Bessel function J_0 is a function of $\Theta \equiv |\nabla S(\psi,\theta)|v_\perp/\Omega$ where $\Omega = Z_j eB_0/m_j c$ is the cyclotron frequency. The perturbed electrostatic potential, once transformed by the "ballooning representation" leads to the eigenfunction $\tilde{\phi}(\theta)$, and its "amplitude" $\hat{\phi}(\theta)$.

A straightforward evaluation of the poloidal derivatives in Eq. (18) follows leading to the final form of the dispersion equation (a second order ordinary differential equation for $\tilde{\phi}$). Its form is given in the Appendix; here we simply note that the velocity integrals can be performed analytically (reduced to Z-functions [50], or to Dawson's integrals as shown in Ref. [38]) since we neglect trapped ion effects (or, equivalently, we ignore the poloidal modulation of $v_\parallel$). This equation is then solved numerically by expansion in a set of basis functions and diagonalization of the resulting determinant (examples of such a procedure can be found in Refs. [51]-[52]; here we use the same expansion in terms of Hermite functions). In all that follows we choose the surface $\Psi = 0.3$ as a reference flux surface; in a plasma with circular cross section this corresponds to $r/a \approx 0.4$ (and $r_B/a \approx 0.37$ for $q(a) = 3$). Note that the equivalent Shafranov

shift (cf. ψ_1 in Sec. 2) will be quite small in low-β JET plasmas: $\psi_1 / \psi_0 \sim r_B / R \approx 0.1$. We will also fix $\rho_i / r_B \approx 0.01$; this value is typical for high temperature experiments (e.g., JET); also $L_{ni} / R = 0.33$, which is characteristic of JET (or any machine with a density profile that is parabolic and aspect ratio near 3). Finally, we take $q_0 = 1$ for illustration, since most of the dependence on this parameter can be compensated by a shift in toroidal mode number ($nq_0 =$ constant).

Fig. 3 shows the ITG modes, with even and odd parity in θ, as a function of the toroidal mode number n (the only good "quantum" number in the problem) for a single-ion plasma. As expected, the mode growth rate peaks for perpendicular wavenumbers that are of the order of an inverse ion Larmor radius: $k_\theta \rho_i \approx 0.3$ (odd mode) and 0.6 (even mode). The odd mode has a somewhat higher frequency of oscillation and, at least for $15 \le n \le 30$, slightly larger growth rate, in qualitative agreement with the fluid results of Sec. 3. The dependence of the mode frequency (real and imaginary part) on the temperature gradient parameter, η_i, is shown in Fig. 4, showing how the mode frequency tracks $\omega_{*Ti} = \eta_i \omega_{*i}$. As a result, the growth rate turns over, after reaching a maximum, for very large values of η_i: the mode decouples from both the sound wave and the precession of the ions (ω_{di}) and growth is turned off (cf. Ref. [6]).

Turning to the effects of ellipticity, we consider Fig. 5, which repeats Fig.4 but for varying degrees of ellipticity. As can be clearly seen, the odd parity mode is essentially unaffected, while the even parity mode is strongly stabilized by vertical elongation. The primary cause can be traced to the effect elongation has on the components (k_r and k_θ) of the "equivalent" wavevector, $\mathbf{k}_\perp(\theta) \equiv \hat{b} \times \nabla S$ (which occurs in the precession drift frequency, the diamagnetic frequency and , in absolute value, as an argument of the Bessel functions in, e.g., Eq. (18)): elongating the cross section tends to yield smaller values of k_r and k_θ at the midplane and larger values at the top and bottom. Note (cf., the local theory, Eq. (17)) that we expect the growth rate to vary with $\omega_{di} \propto \omega_{*i} \propto k_\theta$. As a consequence, the even parity mode (which is weighted principally at the midplane) is "walked down" in $k_\theta \rho_i$ (cf., the curves in Fig. 3) to lower growth rates. The odd parity mode, instead, tends to weight the region with $\theta \approx \pi / 4$ more heavily. In this region, $k_\theta \rho_i$ is largely insensitive to the elongation and the mode is unaffected. Since collisionless trapped electron modes (e.g., the "ubiquitous" mode of Ref. [43]) tend to also appear with $k_\theta \rho_i \approx 1$ we expect that elongation will also have a

stabilizing influence on them. Indeed, elongation was found to produce a mild reduction in the linear growth rate of the dissipative trapped electron mode [53].

The geometric effect of a Shafranov shift can be examined by including the effect of ψ_1, cf. Sec. 2. As indicated earlier, we expect this shift to be small in Ohmic and low power RF heated discharges in JET, but one can do a case study by using Eq. (10), replacing the factor $\pi r_B / 2R_0$ by a varying constant, δ_1. We have performed this analysis and found a stabilizing effect on both modes. This geometric effect is due to the increase in effective $k_r(\theta)\rho_i$ which leads to a modulation (decrease) of the ion driving term by the Bessel functions. This trend is in agreement with that found by Rewoldt et al. [51] (cf. their Sec. III A, where they mention the stabilization due to the θ-variation of the magnetic drift velocity components). The cos θ modulation by these terms causes the odd parity mode to be affected more strongly than the even parity mode(for $\eta_i = 3$ and $n^0q = 30$, a variation of δ_1 from 0 to 0.3 is sufficient to stabilize the odd mode, while the even mode has its growth rate decreased by 48%), as expected (the θ modulation of k_θ is present here as well). For the parameters of interest $\delta_1 \sim 0.1$, the effect is far smaller (γ decrease by 10% for the even mode, 30% for the odd mode).

Fig. 6 shows the case where we vary triangularity (we turn ellipticity off for this case study). The results qualitatively repeat the case for varying ellipticity, though the effect is smaller for the even mode and slightly more pronounced for the odd mode. Here, the weighting of ∇S is done at $\theta = \pm\pi/3$, causing the small difference. Since, in addition, ellipticity is expected to be rather small in the inner plasma region, we shall not consider finite δ_3 any further.

We now come to the effect of having an impurity in the plasma. Note that we choose to peak the impurity density relative to the principal ion: $L_{nI} = L_{ni} / Z_I$ (the principal ion is taken to be hydrogen, for illustration). This is motivated by classical transport theory (see, e.g., the review by Isler [54]) which predicts this peaking: the ion-impurity friction force vanishes for this ratio of density scale lengths. This choice of ratio also automatically entails that $\omega_{*I} = \omega_{*i}$; thus there will be no effects (on the linear modes) due to differential diamagnetic drifts (there is, however, a difference in the effective particle "drift frequency", $\omega_{*j}^T(E, \eta_j)$). In actual situations, data on the steady-state radial profile of n_I is seldom obtained. Profiles for Z_{eff} have been re-constructed and cases with and without peaked Z_{eff} (r) have been published. We keep the main ion parameters (e.g., $L_{ni} / R, \eta_i$) fixed when varying the impurity concentration. This is in order

to isolate the direct effect that the impurity species has on the mode. We choose equal temperatures for all species in the plasma (electrons and ions) for simplicity; this entails that $\eta_I = \eta_i / Z_I << \eta_i$. Thus, impurity driven toroidal ITG instabilities will be rather weak. Equal temperatures can be expected in the central region of the plasma, though high temperature, auxiliary heated experiments commonly have dissimilar electron and ion temperatures.

We immediately see that impurities tend to lower the growth rate of the toroidal ion temperature gradient modes (both even and odd parity branches, cf. Fig. 7) by a combination of dilution of the primary fuel $(n_i = n_e - Z_I n_I)$ and their modification of the mode-particle resonance (in this case, a resonance with the precessing ions, different from "standard" Landau damping). This picture holds for almost all cases, the exception being even parity modes in low-η_i plasmas (cf. the case with η_i = 1 in Fig. 8) for which a small impurity concentration can have a slight destabilizing effect: initially, an addition of impurity ions tends to lower the mode frequency; if this frequency is not much greater than the transit frequency of the primary ions, the growth rate can be temporarily enhanced by the stronger resonant interaction that ensues. We regard this as a "quirk" that occurs in a region where our frequency ordering $(|\omega| >> k_\parallel \upsilon_{Ti})$ is only marginally satisfied, and which may not occur in a more complete calculation. From Fig. 7 one sees that dilution is the primary effect: the curves for Beryllium and Oxygen are very close together when the impurity is singly charged, indicating little selection by mass. On the other hand, the curves for fully ionized impurities (Z_I = 4, and 8, respectively) are lower and further apart, showing the dominant effect of dilution. The odd parity mode is affected more, given its lower initial growth rate and its tendency to be influenced by the mode-particle resonance $\left(\omega - \omega_{Dj}(E,\mu)\right)$ more strongly. Since the odd parity mode has somewhat higher frequency that the even parity branch, more particles resonate with the wave (the argument of the plasma dispersion function is $\xi_\perp \equiv \sqrt{\omega / \omega_{dj} - \upsilon_\perp^2 / \upsilon_{Tj}^2}$, cf. the Appendix, thus only a portion of phase space, $\upsilon_\perp \le \upsilon_{\perp,c}$ is resonant for a given mode frequency).

It is this sensitivity to changes in the resonant contributions within the reponse of the main ion and the impurities that cause the stabilization of the odd parity branch, as opposed to a (large) reduction of the growth rate of the even parity branch (cf. Fig. 8). Note that, as the impurity concentration is increased, the dilution process robs the mode of its main source of free energy (the primary ion) and simultaneously lowers its oscillation frequency, enhancing the resonance

(ions of lower energy become resonant). In general, our results tend to agree with those of Ref. [39], where the dilution process was emphasized.

5. CONCLUSIONS

In this paper, the linear stability of electrostatic ion temperature gradient modes is examined, for shaped toroidal plasmas (in particular, we consider elliptical cross sections) that contain impurities. The specific case of a two-ion plasma (a main ion + one impurity) is studied and linear properties of the toroidal ion temperature gradient (ITG) modes are analyzed in the limit where $k_\parallel v_{Ti} < \omega$. This limit is generally relevant to the toroidal ITG branch, which has its maximum growth rate in the neighborhood $k_\perp \rho_i \sim 1$. Thus, $\omega / k_\parallel v_{Ti} > \omega_{di} / k_\parallel v_{Ti} \approx q k_\perp \rho_i$. The so-called "ballooning formalism" is employed, since we are describing modes with large nq (n is the toroidal mode number and q is the inverse rotational transform). Attention is payed to the comparison between the even and odd parity (in θ) branches of the instability. The odd branch is a "pure" ITG mode (modes that are odd in θ average out the trapped electron response, to lowest order in the ratio of the mode frequency to the electron bounce frequency, and, thus, cannot be driven unstable by them). The even parity branch, on the other hand, feels the effect of trapped electrons and can tap their free energy (i.e., their temperature gradient) as well as that of the ions (cf. [43]). Thus, the concept of a "threshold value" for $\eta_i \equiv d \ln T_i / d \ln n_i$ is really meaningful only for the odd parity branch. As was clearly illustrated by Rewoldt, Tang, and Frieman (cf. Fig. 5 of Ref. [55]) the instability of the ITG mode connects *in a continuous fashion* with that of the trapped electron mode: as η_i is lowered to (and past) zero, the mode goes from rotating in the ω_{*i} direction to rotating in the ω_{*e} direction with a decreasing, though finite, growth rate. In this work, we ignore trapped electrons, so as to isolate effects due purely to ion temperature gradients.

Having said this, the main results of the present research are two-fold. Toroidicity (in the sense of a Shafranov shift of the magnetic flux surfaces, as opposed to the magnetic precession drift which drives the instability) tends to lower the growth rate of both even and odd parity modes, with the odd parity mode being measurably affected even in cases where the shift is small $(\psi_1 / \psi_0 \sim 0.1)$. Ellipticity has a stabilizing effect on the even parity mode, but leaves the odd parity mode essentially unaffected (triangularity has a much smaller, stabilizing effect, affecting even and odd modes roughly equally at

maximum growth). One can quickly generalize this result to cover the trapped electron mode ("ubiquitous"): it will behave exactly as the even ITG root. The presence of an impurity species, on the other hand, tends to affect the odd ITG root more strongly than the even root. Still, both roots tend to be stabilized by the presence of impurities, mostly due to a dilution of the concentration of the principal ion ($n_i = n_e - Z_I n_I$, for hydrogenic main ions). As the impurity concentration is raised, the mode oscillation frequency and its growth rate decrease, thus our calculation may actually underestimate the stabilizing effect somewhat, as it assumes that $k_\| v_{Ti} < \omega$. In any case, we find that the only important "selection" is by impurity charge (as opposed to mass, singly ionized impurities have effects that are quantitavely almost identical). As long as the impurity is "light" (e.g., Beryllium), we do not have to worry about impurity driven modes (cf. Ref. [40]-[41]): the impurity-ITG mode (due to η_i) will not be active for peaked impurity density profiles ($\eta_I = (L_{nI} / L_{nI})\eta_i$ is small for $L_{nI} = L_{ni} / Z_I$) provided the impurity is fully ionized. The impurity drift wave (cf. [35], [56], [57]) will not contribute either for light impurities, as its window of instability in parameter space nearly vanishes (see, e.g., Refs. [40] and [56]).

An analysis of marginal stability properties of these modes is highly desirable [M. Ottaviani, private communication], especially for the odd parity mode (for which the concept of a critical η_i is meaningful). Unfortunately, this objective cannot be achieved using the present dispersion equation, Eq. (18). As the temperature gradient parameter is lowered, in our study, the mode frequency (as well as the growth rate) becomes smaller, until it falls below the transit frequency of the primary ion, thereby invalidating our orderings. This points to the necessity of a systematic study that keeps Landau damping effects to all orders. It seems apparent that coupling between the slab and toroidal branches is most important near marginal stability; indeed it may determine the threshold. For the modes that are amendable to this analysis (i.e., high toroidal mode number odd parity modes which have large real frequencies), the threshold value of η_i is indeed raised by factors of order $Z_I n_I / n_e$ (e.g. $\eta_{i,crit}$, goes from 1.45 to 2.0 for the n = 55 odd parity mode, as the impurity concentration is raised to $Z_I n_I / n_e$ = 0.12). This trend is stronger than the increase in threshold temperature gradient found in Ref. [19] (see their Fig. 1, which turned off both FLR and the sound wave; the latter effect is in our opinion the major cause of the difference). The analysis of Ref. [39] is not amenable to a comparison (the authors of that work find a non-monotonic dependence of the threshold value of L_T/R on impurity concentration), as they include collsional trapped electron dynamics, treat the

impurities as a fluid, and approximate the resonant denominator in the primary ion response by making the precession frequency a function of energy alone.

The consequences for experiments are as follows: the concept of "measuring" a critical L_{Ti} (via the parameter η_i or in the ratio L_{Ti}/R) by considering energy transport across the plasma column is by no means straighforward. We have noted that both parity branches of the ITG instability are affected (stabilized) by the presence of multiply charged impurities (dilution effect). Thus, any comparison with theory must account for the presence of impurities, rather than employing values of $\eta_{i,crit}$ computed for pure plasmas (cf., Fig.3 of Ref. [30], and Fig. 5 of Ref. [31]). Secondly, at least one branch (the even parity branch) can employ the trapped electron channel to become unstable and affect the ion as well as the electron energy fluxes (cf. Fig. 7 of Ref. [58]). Thus, any experimental effort toward resolving the origin of the anomalous energy transport would benefit from a determination of the parity (about the midplane) of the modes that produce the observed microturbulance.

Note added: At the time this manuscript was being accepted for publication, a paper by Hua, Xu and Fowler appeared in print [59]. That paper deals with the effect of ellipticity on the even parity modes in pure $(Z_{eff} = 1)$ plasmas. It too shows the stabilization by increasing ellipticity.

ACKNOWLEDGMENTS

This research was begun while the author was a visitor at JET (the author wishes to thank D. Düchs for his kind hospitality) and was concluded at MIT under the sponsorship of the U.S. Department of Energy, under task DE-FG02-91ER-54109. Numerical computations were carried out at JET and at the National Energy Research Supercomputer Centre (Livermore). The author wishes to thank M. Ottaviani for a critical reading of the manuscript and several fruitful suggestions.

APPENDIX

Here we give the specific form of the dispersion equation which we solve. We choose to express it in terms of the plasma dispersion function, Z (cf. [50]). The alternative is to use a form involving Dawson's intergral (cf. [38]), which must be evaluated numerically anyway. The equation reads:

$$\left(1+\sum_{j\neq e}\frac{Z_j^2 n_j}{n_e}\frac{T_e}{T_j}\right)\frac{e\hat{\phi}(\theta)}{T_e}+\sum_{j\neq e}\frac{Z_j^2 n_j}{n_e}\frac{T_e}{T_j}\Bigg\{-\eta_j\xi_{*j}\Gamma_{0j}$$

$$+2\int_0^\infty dy\ y\ \exp\left(-y^2\right)J_0^2\left(y\sqrt{b_j}\right)\left[\xi_j-\xi_{*j}\left(1-\eta_j\left(3/2-y^2\right)\right)\right] \qquad \text{(A-1)}$$

$$-\eta_j\xi_{*j}\xi_\perp^2\Big]\frac{1}{\xi_\perp}Z(\xi_\perp)+\frac{\upsilon_{T_j}^2}{8J^2B^2\omega_{dj}^2}\left[L_{0j}+L_{1j}\frac{d}{d\theta}+L_{2j}\frac{d^2}{d\theta^2}\right]\Bigg\}\frac{e\hat{\phi}(\theta)}{T_e}=0$$

where the purturbed electrostatic potential is related to its "amplitude" by $\tilde{\phi}(r,\theta,\phi)=\exp\left[iS(r,\theta,\phi)\right]\hat{\phi}(\theta)$, S is the eikonal introduced in Sec. 4, J is the Jacobian defined in Sec. 2, $y\equiv\upsilon_\perp/\upsilon_{Tj}$ is a dimensional velocity variable, $\xi_j\equiv\omega/\omega_{dj}$ and $\xi_{*j}\equiv\omega_{*j}/\omega_{dj}$ are dimensionaless frequencies and, $\xi_\perp\equiv\sqrt{\xi_j-y^2}$. The finite Larmor radius parameter is $b_j\equiv\left(|\nabla S|\upsilon_{Tj}/\Omega_j\right)^2$ and $\Gamma_{0j}\equiv I_0\left(b_j/2\right)\exp\left(-b_j/2\right)$ while the temperature gradient is characterized by $\eta_j\equiv\left(d\ln T_j/dr\right)/\left(d\ln n_j/dr\right)$. The three coefficient L_{Nj} are given below; the coefficient of the second derivative is:

$$L_{2j}=-2\int_0^\infty dy\ y\ \exp\left(-y^2/2\right)J_0^2\frac{1}{\xi_\perp^3}\Big\{\Big[\left(\xi_\perp^2-1/2\right)Z^{(2)}-2Z\Big]\Big[\xi_j-\xi_{*j}(1$$

$$-\eta_j\left(3/2-y^2\right)\Big)\Big]-\eta_j\xi_{*j}\xi_\perp^2\Big[\left(\xi_\perp^2-5/2\right)Z^{(2)}-2Z\Big]\Big\} \qquad \text{(A-2)}$$

Here $Z(\xi_\perp)$ is the plasma dispersion function and $Z^{(N)}$ is its N-th derivative. The first derivative coefficient is written as $L_{1j}=L_{1j1}+L_{1j2}$, where:

$$L_{1j1}=6\int_0^\infty dy\ y\ \exp\left(-y^2/2\right)J_0\left[2y\left(\rho_j\frac{\partial|\nabla S|}{\partial\theta}\right)J_1+\left(\frac{\partial\ln J}{\partial\theta}+\frac{\partial\ln\omega_{di}}{\partial\theta}\right)J_0\right]$$

$$\times\frac{1}{\xi_\perp^3}\Big\{\Big[\big(\xi_\perp^2-1/2\big)Z^{(2)}-2Z\Big]\Big[\xi_j-\xi_{*j}\big(1-\eta_j\big(3/2-y^2\big)\big)\Big]$$
$$-\eta_j\xi_{*j}\xi_\perp^2\Big[\big(\xi_\perp^2-5/2\big)Z^{(2)}-2Z\Big]\Big\} \tag{A-3}$$

$$L_{1j2}=\left(\xi_j\frac{\partial\ln\omega_{dj}}{\partial\theta}\right)\int_0^\infty dy\ \ y\ \exp\big(-y^2/2\big)J_0^2\frac{1}{\xi_\perp^5}\Big\{\Big[\xi_\perp^3Z^{(3)}-\big(3\xi_\perp Z^{(1)}-Z\big)\Big]\Big[\xi_j$$
$$-\xi_{*j}\big(1-\eta_j\big(3/2-y^2\big)\big)\Big]-\eta_j\xi_{*j}\xi_\perp^2\Big[\xi_\perp^3Z^{(3)}+6\xi_\perp^2Z^{(2)}+3\big(\xi_\perp Z^{(1)}-Z\big)\Big]\Big\} \tag{A-4}$$

The last coefficient is split into three pieces, $L_{0j} = L_{0j1} + L_{0j2} + L_{0j3}$, where

$$L_{0j1}=2\int_\theta^\infty dy\ \ y\ \exp\big(-y^2/2\big)J_0\Big\{\Big[y^2\Big(\rho_j\frac{\partial|\nabla S|}{\partial\theta}\Big)^2+\frac{1}{\omega_{dj}}\frac{\partial^2\omega_{dj}}{\partial\theta^2}-\frac{\partial\ln J}{\partial\theta}\frac{\ln\omega_{dj}}{\partial\theta}$$
$$-3\Big(\frac{\partial\ln\omega_{dj}}{\partial\theta}\Big)^2\Big]J_0-y|\nabla S|\rho_j\Big[\Big(\frac{\partial\ln|\nabla S|}{\partial\theta}\Big)^2-\frac{1}{|\nabla S|}\frac{\partial^2|\nabla S|}{\partial\theta^2}$$
$$+\frac{\partial\ln|\nabla S|}{\partial\theta}\frac{\partial\ln J}{\partial\theta}+3\frac{\partial\ln|\nabla S|}{\partial\theta}\frac{\partial\ln\omega_{dj}}{\partial\theta}\Big]J_1\Big\}\frac{1}{\xi_\perp^3}\Big\{\Big[\big(\xi_\perp^2-1/2\big)Z^{(2)}-2Z\Big]$$
$$\times\Big[\xi_j-\xi_{*j}\big(1-\eta_j\big(3/2-y^2\big)\big)\Big]-\eta_j\xi_{*j}\xi_\perp^2\Big[\big(\xi_\perp^2-5/2\big)Z^{(2)}-2Z\Big]\Big\} \tag{A-5}$$

$$L_{0j2}=-\xi_j\int_0^\infty dy\ \ y\ \exp\big(-y^2/2\big)J_0\Big\{\Big[\frac{\partial\ln\omega_{dj}}{\partial\theta}\Big(2\frac{\partial\ln\omega_{dj}}{\partial\theta}+\frac{1}{3}\frac{\partial\ln J}{\partial\theta}\Big)-\frac{1}{3\omega_{dj}}\frac{\partial^2\omega_{dj}}{\partial\theta^2}\Big]J_0$$
$$+yp_j\frac{\partial|\nabla S|}{\partial\theta}\frac{\partial\ln\omega_{dj}}{\partial\theta}J_1\Big\}\frac{1}{\xi_\perp^5}\Big\{\Big[\xi_\perp^3Z^{(3)}-\big(3\xi_\perp Z^{(1)}-Z\big)\Big]\Big[\xi_j-\xi_{*j}\big(1-\eta_j\big(3/2-y^2\big)\big)\Big]$$
$$-\eta_j\xi_{*j}\xi_\perp^2\Big[\xi_\perp^3Z^{(3)}+6\xi_\perp^2Z^{(2)}+3\big(\xi_\perp Z^{(1)}-Z\big)\Big]\Big\} \tag{A-6}$$

$$L_{0j3}=-\Big(\frac{\xi_j}{4}\frac{\partial\ln\omega_{dj}}{\partial\theta}\Big)^2 2\int_0^\infty dy\,y\exp\big(-y^2/2\big)J_0^2\frac{1}{\xi_\perp^7}\Big\{\Big[\xi_\perp^4Z^{(4)}-2\xi_\perp^3Z^{(3)}$$
$$-3\big(\xi_\perp^2+5/2\big)Z^{(2)}-30Z\Big]\Big[\xi_j-\xi_{*j}\big(1-\eta_j\big(3/2-y^2\big)\big)\Big] \tag{A-7}$$
$$-\eta_j\xi_{*j}\xi_\perp^2\Big[\xi_\perp^4Z^{(4)}+6\xi_\perp^3Z^{(3)}-3\big(\xi_\perp^2-3/2\big)Z^{(2)}+18Z\Big]\Big\}$$

REFERENCES

[1] L.I. Rudakov and R.Z. Sagdeev, Sov. Phys. Dokl. **6**, 415 (1961).

[2] B. Coppi, M.N. Rosenbluth, and R.Z. Sagdeev, Phys. Fluids **10**, 582 (1967).

[3] T.M. Antonsen, Jr., B. Coppi, and R.C. Englade, Nucl. Fusion **19**, 681 (1979).

[4] P.N. Guzdar, L. Chen, W.M. Tang, and P.H. Rutherford, Phys. Fluids **26**, 673 (1983).

[5] Y.K. Pu and S. Migliuolo, Phys. Fluids **28**, 1722 (1985).

[6] S. Migliuolo, Phys. Fluids **28**, 2778 (1985).

[7] S. Migliuolo, Phys. Fluids **30**, 922 (1987).

[8] S. Migliuolo, J. Geophys. Res. **93**, 867 (1988).

[9] S. Migliuolo, Phys. Lett. **A131**, 373 (1988).

[10] O. Mathey and A.K. Sen, Phys. Rev. Lett. **62**, 268 (1989).

[11] S. Migliuolo, and A.K. Sen, Phys. Fluids **B2**, 3047 (1990).

[12] G.M. Staebler and R.R. Dominguez, Nucl. Fusion **31**, 1891 (1991).

[13] W. Horton, D.I. Choi, and W.M. Tang, Phys. Fluids **24**, 1077 (1981).

[14] W. Horton, D.I. Choi, and B.G. Hong, Phys. Fluids **26**, 1641 (1983).

[15] W. Horton, J.E. Sedlak, D.I. Choi, and B.G. Hong, Phys. Fluids **28**, 3050 (1985).

[16] J.Y. Kim and W. Horton, Phys. Fluids **B3**, 1167 (1991).

[17] J.Y. Kim, W. Horton, D.I. Choi, S. Migliuolo, and B. Coppi, Phys. Fluids **B4**, 152 (1992).

[18] R.E. Waltz, W. Pfeiffer, and R.R. Dominguez, Nucl. Fusion **20**, 43, (1980).

[19] R.R. Dominguez, and R.E. Waltz, Phys. Fluids **31**, 3147 (1988).

[20] A. Jarmen, P. Anderson, and J. Weiland, Nucl. Fusion **27**, 941, (1987).

[21] J. Nillson, M Liljeström, and J. Weiland, Phys. Fluids **B2**, 2568 (1990).

[22] F. Romanelli, Phys. Fluids **B1**, 1018 (1989).

[23] M. Ottaviani, F. Romanelli, R. Benzi, M. Briscolini, P. Santangelo, and S. Succi, Phys. Fluids **B2**, 67 (1990).

[24] N. Mattor and P.H. Diamond, Phys. Fluids **B1**, 1980 (1989).

[25] X.Q. Xu and M.N. Rosenbluth, Phys. Fluids **B3**, 627 (1991).

[26] J.P. Mondt and J. Weiland, Phys. Fluids **B3**, 3248 (1991).

[27] S.M. Wolfe, M. Greenwald, R. Gandy, R. Granetz, C. Gomez, D. Gwinn, B. Lipschultz, S. McCool, E. Marmar, J. Parker, R.R. Parker, and J. Rice, Nucl. Fusion **26**, 329 (1986).

[28] O. Gehre, O. Gruber, H.D. Murmann, D.E. Roberts, F. Wagner, B. Bomba, A. Eberhagen, H.U. Fahrbach, G. Fussmann, J. Gernhardt, K. Hubner, G. Janschitz, K. Lackner, E.R. Muller, H. Niedermeyer, H. Rohr,

G. Staudenmeier, K.H. Steuer, and O. Vollmer, Phys. Rev. Lett. **60**, 1502 (1988).

[29] F.X. Soldner, E.R. Muller, F. Wagner, H.S. Bosch, A. Eberhagen, H.U. Fahrbach, G. Fussmann, O. Gehre, K. Gentle, J. Gernhardt, O. Gruber, W. Herrmann, G. Janeschitz, M. Kornherr, H.M. Mayer, K. McCormick, H.D. Murmann, J. Neuhauser, R. Notle, W. Poschenrieder, H. Rohr, K.H. Steuer, U. Stroth, N. Tsois, and H. Verbech, Phys. Rev. Lett. **61**, 1105 (1988).

[30] A. Taroni, F. Tibone, B. Balet, D. Boucher, J.P. Christiansen, J.G. Cordey, G.C. Corrigan, D.F. Düchs, R. Giannella, A. Gondhalekar, N. Gottardi, G.M.D. Hogeweij, L. Lauro-Taroni, K. Lawson, M. Mattioli, D. Muir, J.O'Rourke, D. Pasini, P.H. Rebut, C. Sack, G. Sips, E. Springmann, T.E. Stringer, P. Stubberfield, K. Thomsen, M.L. Watkins, and H. Wiesen, in *Plasma Physics and Cont. Nuclear Fusion Research 1990* (IAEA, Vienna), vol. 1, p. 93 (1991).

[31] M.C. Zarnstorff, C.W. Barnes, P.C. Efthimion, G.W. Hammett, W. Horton, R.A. Hulse, D.K. Mansfield, E.S. Marmar, K.M. McGuire, G. Rewoldt, B.C. Stratton, E.J. Synakowski, W.M. Tang, J.L. Terry, X.Q. Xu, M.G. Bell, R.J. Fonck, E.D. Fredrickson, H.P. Furth, R.J. Goldston, B. Grek, R.J. Hawryluk, K.W. Hill, H. Hsuan, D.W. Johnson, D.C. McCune, D.M. Meade, D. Mueller, D.K. Owens, H.K. Park, A.T. Ramsey, M.N. Rosenbluth, J. Schivell, G.L. Schmidt, S.D. Scott, G. Taylor, and R.M. Wieland, in *Plasma Physics and Cont. Nuclear Fusion Research 1990* (IAEA, Vienna), vol. 1, p. 109 (1991).

[32] K.H. Burrell, R.J. Groebner, T.S. Kurki-Suonio, T.N. Carlstrom, R.R. Dominguez, P. Gohil, R.A. Jong, H. Matsumoto, J.M. Lohr, T.W. Petrie, G.D. Porter, G.T. Sager, H.E. St. John, D.P. Schissel, and S.M. Wolfe, in *Plasma Physics and Cont, Nuclear Fusion Research 1990* (IAEA, Vienna), vol. 1, p. 123 (1991).

[33] W. Horton, D. Lindberg, J.Y. Kim, J.Q. Dong, G.W. Hammett, S.D. Scott, M.C. Zarnstorff, and S. Hamaguchi, Physics of Fluids **B4**, 953 (1992).

[34] X. Garbet, L. Laurent, F. Mourgues, J.P. Roubin, A. Samain, X.L. Xou, and J. Chinardet, in *Proc. 18th Europ. Conf. on Cont. Fusion and Plasma Heating,* vol. 15C, pt. 4, p. 21 (1991).

[35] B. Coppi, H.P. Furth, M.N. Rosenbluth, and R.Z. Sagdeev, Phys. Rev. Lett. **17**, 377 (1966).

[36] B. Coppi and C. Spight, Phys. Rev. Lett. **41**, 551 (1978).

[37] W.M. Tang, R.B. White, and P.N. Guzdar, Phys. Fluids **23**, 167 (1980).

[38] R.R. Dominguez and M.N. Rosenbluth, Nucl. Fusion **29**, 844 (1989).

[39] R. Paccagnella, F. Romanelli, and S. Briguglio, Nucl. Fusion **30**, 545 (1990).

[40] S. Migliuolo, Nucl. Fusion **32**, 1331 (1992).

[41] M. Fröjdh, M. Liljeström, and H. Nordman, Nucl. Fusion **32**, 419 (1992).
[42] J.P. Freidberg *Ideal Magnetohydrodynamics* (Plenum, NY, 1987).
[43] B. Coppi and F. Pegoraro, Nucl. Fusion **17**, 969 (1977); F. Pegoraro, "Odd Ion Instability Driven by the Magnetic Curvature Drift", MIT/RLE report PRR-76/6 (unpublished).
[44] P.W. Terry, J.N. LeBoeuf, P.H. Diamond, D.R. Thayer, J.E. Sedlak, and G.S. Lee, Phys. Fluids **31**, 2920 (1988).
[45] J.W. Connor, R.J. Hastie, and J.B. Taylor, Proc. Roy. Soc. London **A365**, 1 (1979).
[46] P.H. Rutherford and E.A. Frieman, Phys. Fluids **11**, 569 (1968).
[47] T.M. Antonsen, Jr. and B. Lane, Phys. Fluids **23**, 1205 (1980).
[48] F. Pegoraro and T.J. Schep, Phys. Fluids **24**, 478 (1981).
[49] J.W. Connor, R.J. Hastie, and T.J. Martin, Nucl. Fusion **23**, 1702 (1983).
[50] B.D. Fried and S.E. Conte *The Plasma Dispersion Function* (Academic, NY, 1961).
[51] G. Rewoldt, W.M. Tang, and M.S. Chance, Phys. Fluids **25**, 480 (1982).
[52] B. Coppi, S. Migliuolo, and Y.K. Pu, Phys. Fluids **B2**, 2322 (1990).
[53] K.R. Chu, E. Ott, and W.M. Manheimer, Phys. Fluids **21**, 664 (1978).
[54] R.C. Isler, Nucl. Fusion **24**, 1599 (1984).
[55] G. Rewoldt, W.M. Tang, and E.A. Frieman, Phys. Fluids **23**, 2011 (1980).
[56] B. Coppi, G. Rewoldt, and T. Schep, Phys. Fluids **19**, 1144 (1976).
[57] B. Coppi, in *Plasma Physics and Cont. Nuclear Fusion Research 1990* (IAEA, Vienna), vol. 2, p. 413 (1991).
[58] G. Rewoldt and W.M. Tang, Phys. Fluids **B2**, 318 (1990).
[59] D.D. Hua, X.Q. Xu, and T.K. Fowler, Phys. Fluids **B4**, 3216 (1992).

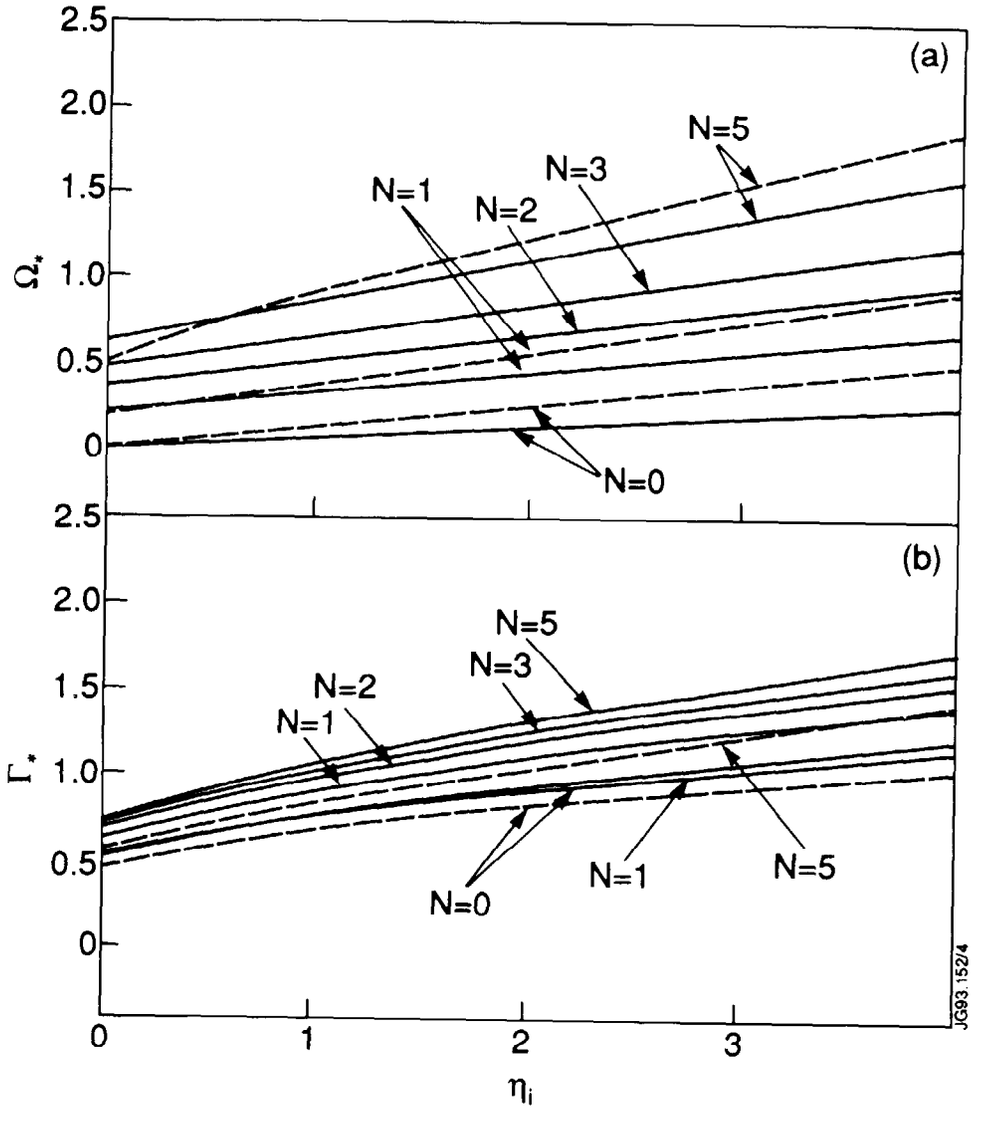

Fig. 1 Normalized eigenfrequency, $\omega / \omega_{*i} = \Omega_* + {}_i\,\Gamma_*$ as a function of the ion temperature gradient parameter, $\eta_i = d\ln T_i / d\ln n_i$. Circular cross section, no impurities, **fluid limit** with the strong coupling approximation, solid (dashed) lines indicate $\bar{b}_i = 0.1\ (0.25)$, N = radial mode number. Parameters are: $L_n / R = 0.125 (\leftrightarrow \varepsilon = 0.25)$, $\hat{s} = 1, c_s / qR\omega_{*i} = (L_n / R) / \sqrt{2\bar{b}_i}$.
(a) oscillation frequency Ω_*, (b) growth rate Γ_*.

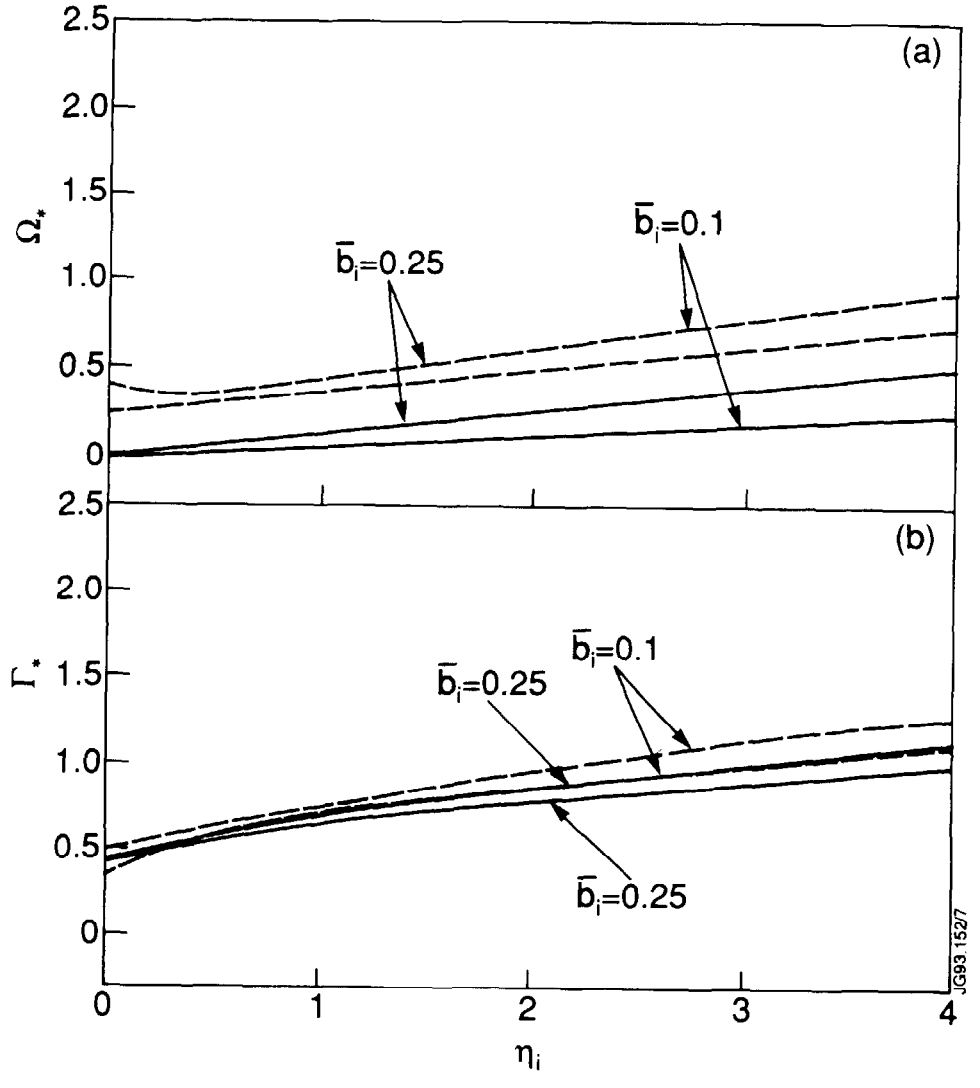

Fig. 2 Normalized eigenfrequency, $\omega / \omega_{*i} = \Omega_* +_i \Gamma_*$ as a function of the ion temperature gradient parameter, $\eta_i = d\ln T_i / d\ln n_i$. Circular cross section, no impurities, **fluid limit** with full harmonic dependence of the precession drift frequency, Parameters are: $L_n / R = 0.125 (\leftrightarrow \varepsilon = 0.25)$, . $\hat{s} = 1, c_s / qR\omega_{*i} = (L_n / R) / \sqrt{2\bar{b}_i}$ Solid (dashed) lines denote even (odd) modes. (a) oscillation frequency Ω_*, (b) growth rate Γ_*.

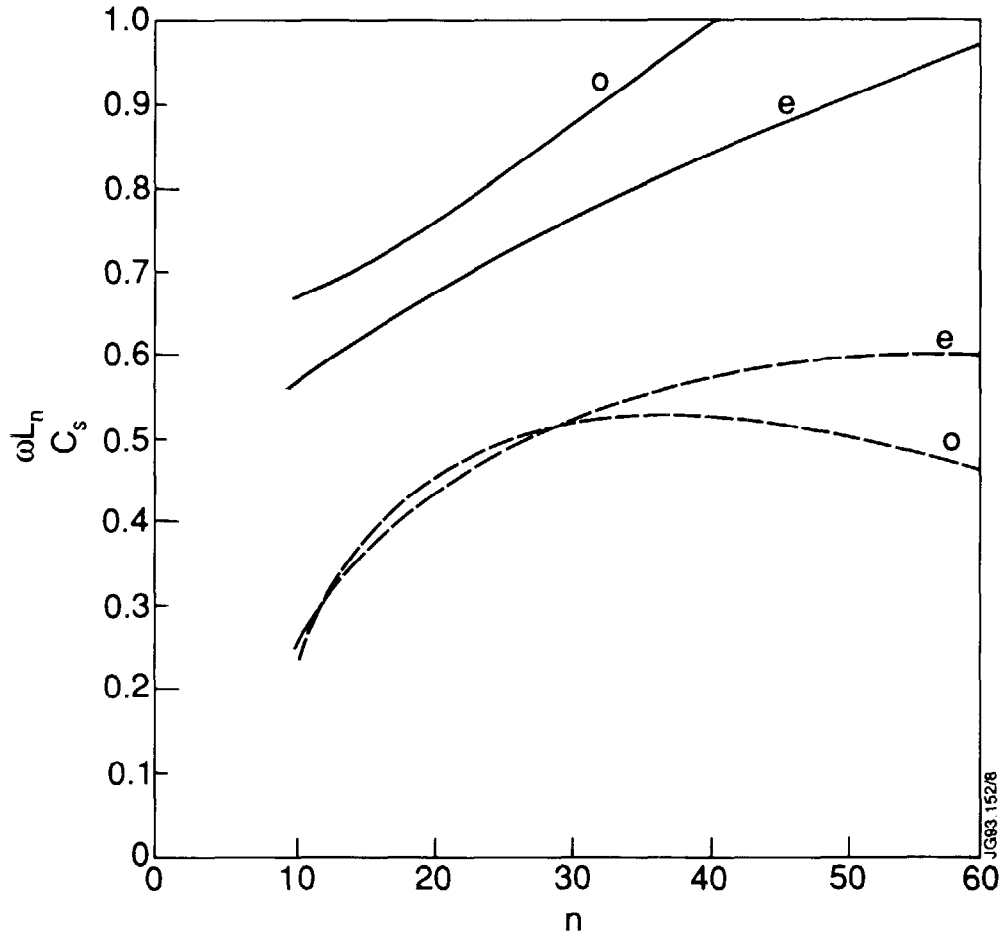

Fig. 3 Normalized eigenfrequency, $\omega L_n / c_s = \Omega + i\,\Gamma$, as a function of the toroidal mode number n; **kinetic theory**, Parameters are: $\Psi = 0.3$, $q_0 = 1$, $\rho_i / r_B = 0.01$, $L_{ni} / R = 0.33$, $\eta_i = 5$, $\delta_j = 0$ (circular cross section), no impurities. Solid (dashed) lines show the oscillation frequency (growth rate); the labels e(o) refer to the even (odd) parity mode.

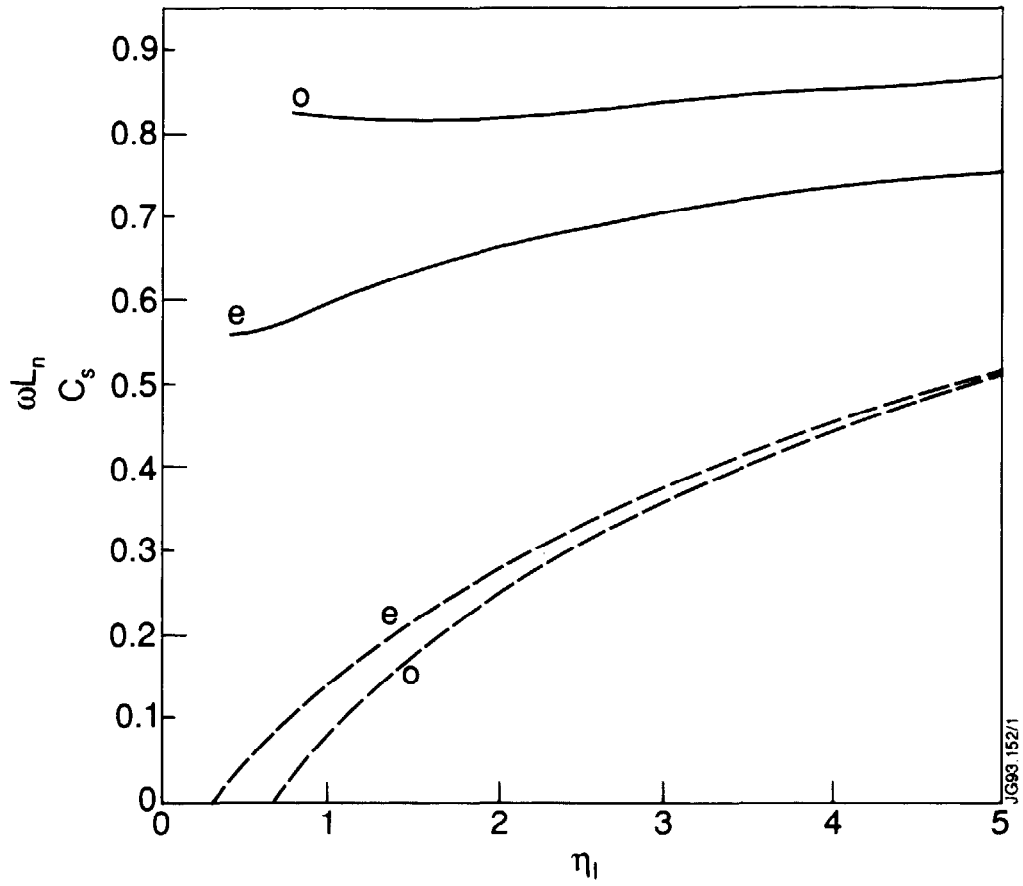

Fig. 4 Normalized eigenfrequency, $\omega L_n / c_s = \Omega +_i \Gamma$, as a function of the temperature gradient η_i; **kinetic theory**. Other parameters are: $\psi = 0.3$, $q_0 = 1$, $\rho_i / r_B = 0.01$, $L_{ni} / R = 0.33$, $n = 30$ (toroidal mode number), $\delta_j = 0$ (circular cross section), no impurities. Solid (dashed) lines show the oscillation frequency (growth rate); the labels e(o) refer to the even (odd) parity mode.

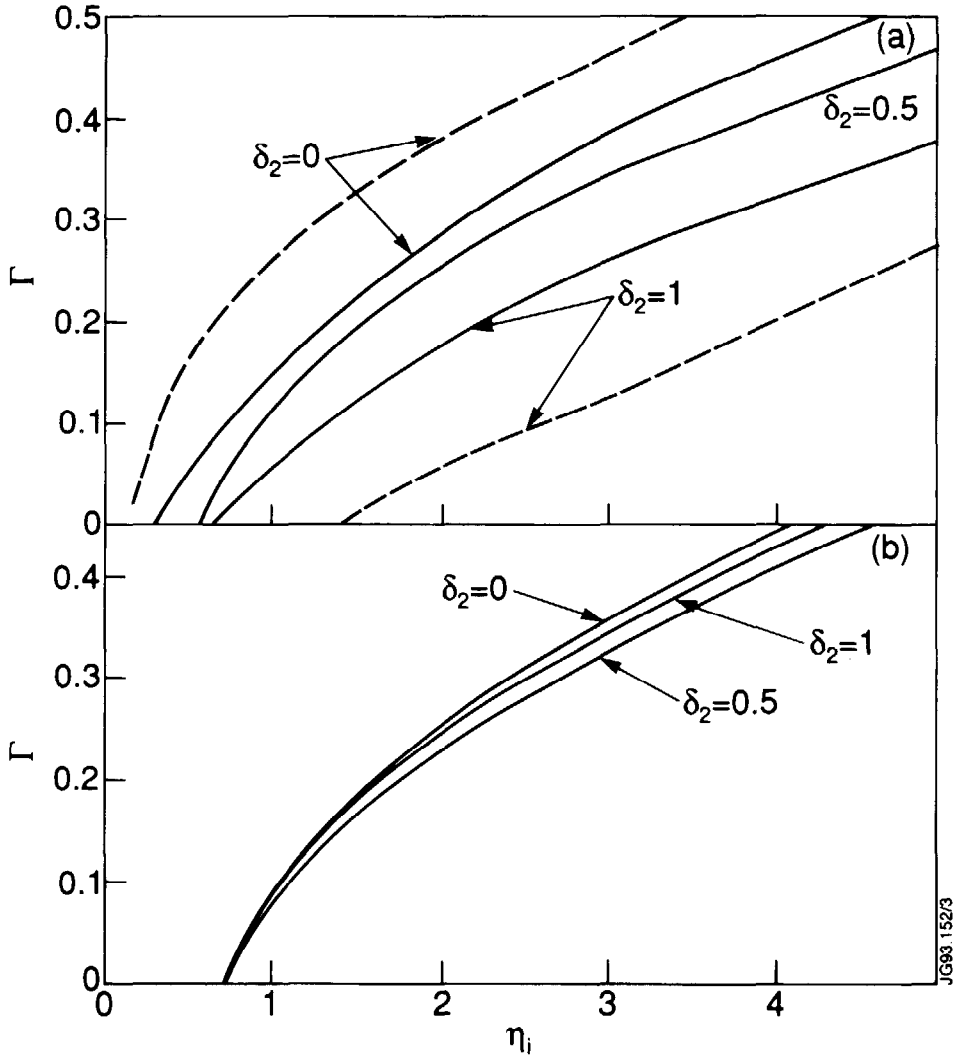

Fig. 5 Normalized growth rate, $\Gamma = \gamma L_n / c_s$, as a function of the temperature gradient parameter η_i (kinetic theory), for various degrees of ellipticity $\delta_2 = 0,0.5,1$ corresponds to k_{ell} = 1,1.29,1.73 near the centre), no triangularity; (a) even mode, solid (dashed) lines denote n = 30(50) (toroidal mode number); (b) odd mode with n = 30. Other parameters are: $\psi = 0.3$, $q_0 = 1$, $\rho_i / r_B = 0.01$, $L_{ni} / R = 0.33$, no impurities.

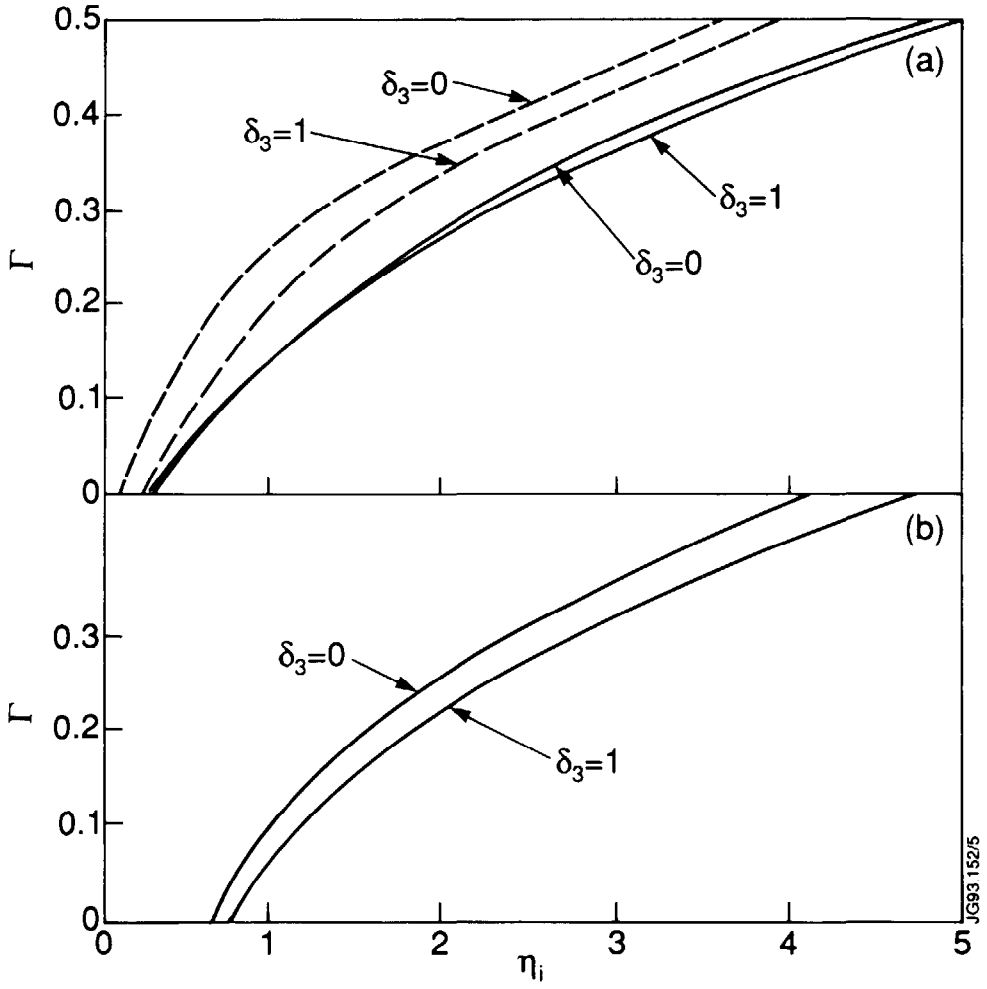

Fig. 6 Normalized growth rate, $\Gamma = \gamma L_n / c_s$, as a function of the temperature gradient parameter η_i (kinetic theory), for various degrees of triangularity $\delta_3 = 0, 0.5, 1$; the ellipticity is turned off for this case); (a) even mode, solid (dashed) lines denote n = 30(50) (toroidal mode number); (b) odd mode with n = 30. Other parameters are $\Psi = 0.3$, $q_0 = 1$, $,\rho_i / r_B = 0.01$, $L_{ni} / R = 0.33$, no impurities.

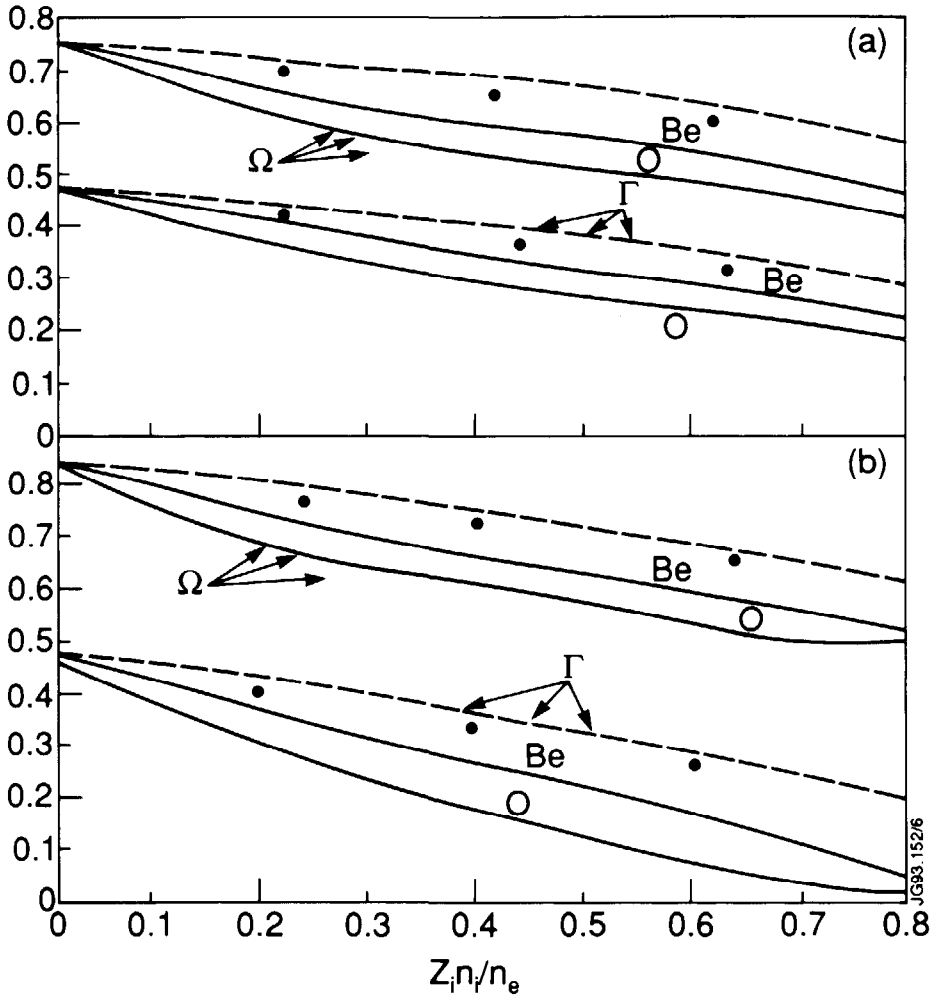

Fig. 7 Normalized eigenfrequency, $\omega L_n / c_s = \Omega + _i \Gamma$, as a function of the impurity concentration $Z_I n_I / n_e$ (kinetic theory), hydrogen plasma; (a) even mode, (b) odd mode. Dashed lines show singly ionized Beryllium (m_I = 9m_H), crosses show singly ionized Oxygen (m_I = 16m_H), solid lines denote fully ionized Beryllium (Z_I = 4) or Oxygen (Z_I = 8). Parameters are: $\psi = 0.3$, $q_0 = 1$, $\delta_2 = 0.44$, $\delta_{j\neq 2} = 0$, $n = 30$, $\rho_i / r_B = 0.01, \eta_i = 5$, $L_{ni} / R = 0.33$, $L_{nI} = L_{ni} / Z_I$ (peaked impurity density profile), $T_e = T_i = T_I$.

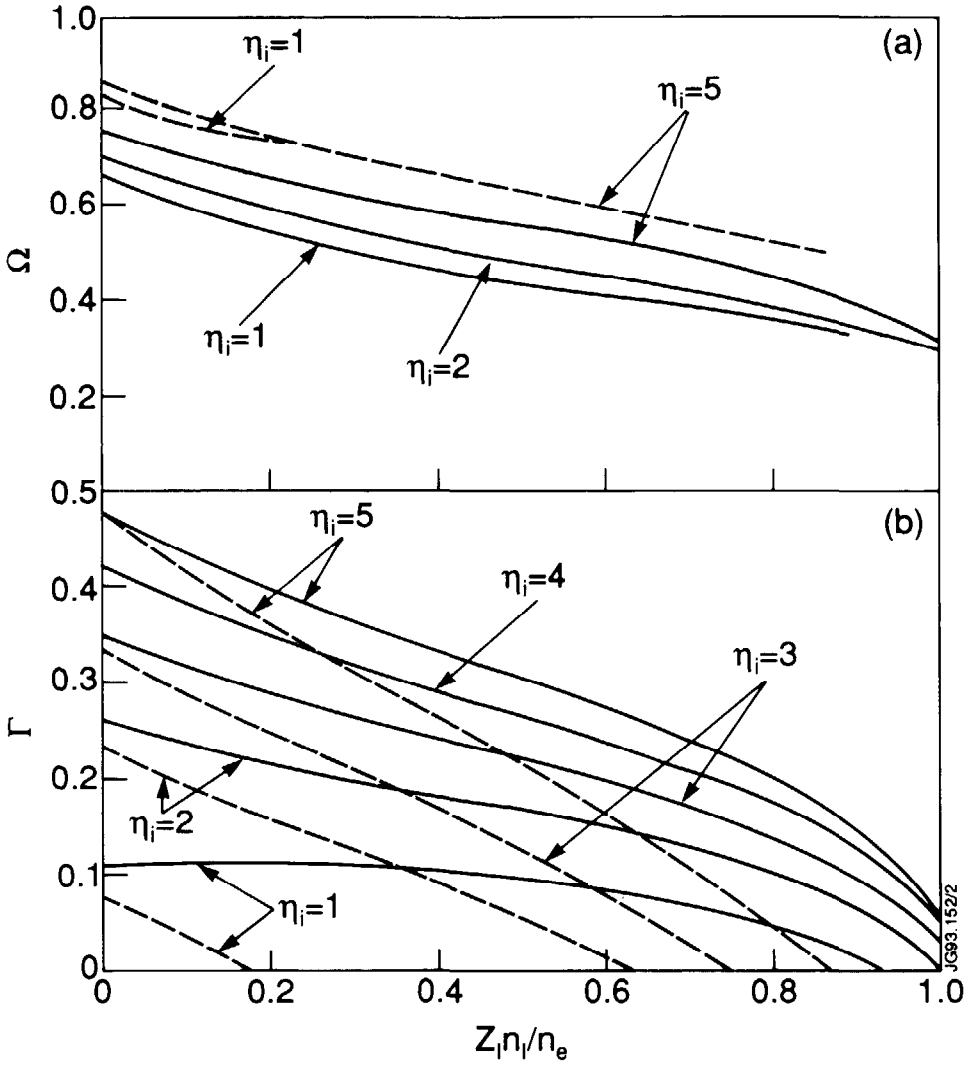

Fig. 8 Normalized eigenfrequency, $\omega L_n / c_s = \Omega + _i \Gamma$, as a function of the impurity concentration $Z_I n_I / n_e$ (kinetic theory), Beryllium in a hydrogen plasma; (a) mode frequency, (b) growth rate. Solid (dashed) lines show the even (odd) parity branch. Parameters are $\psi = 0.3$, $q_0 = 1$, $\delta_2 = 0.44$, $\delta_{j\neq 2} = 0$, $n = 30$, $\rho_i / r_B = 0.01, \eta_i = 5, L_{ni} / R = 0.33$, $L_{nI} = L_{ni} / Z_I$ (peaked impurity density profile), $T_e = T_i = T_I$.